Precession and recession of the rock'n'roller

Peter Lynch and Miguel D Bustamante

School of Mathematical Sciences, UCD, Belfield, Dublin 4, Ireland

E-mail: Peter.Lynch@ucd.ie and Miguel.Bustamante@ucd.ie

Abstract
We study the dynamics of a spherical rigid body that rocks and rolls on a plane
under the effect of gravity. The distribution of mass is non-uniform and the
centre of mass does not coincide with the geometric centre. The symmetric case,
with moments of inertia $I_1 = I_2 < I_3$, is integrable and the motion is completely
regular. Three known conservation laws are the total energy E, Jellett's quantity
Q_J and Routh's quantity Q_R. When the inertial symmetry $I_1 = I_2$ is broken,
even slightly, the character of the solutions is profoundly changed and new
types of motion become possible. We derive the equations governing the
general motion and present analytical and numerical evidence of the recession,
or reversal of precession, that has been observed in physical experiments. We
present an analysis of recession in terms of critical lines dividing the (Q_R, Q_J)
plane into four dynamically disjoint zones. We prove that recession implies
the lack of conservation of Jellett's and Routh's quantities, by identifying
individual reversals as crossings of the orbit $(Q_R(t), Q_J(t))$ through the critical
lines. Consequently, a method is found to produce a large number of initial
conditions so that the system will exhibit recession.

PACS numbers: 45.20.dc, 45.20.Jj, 45.40.Cc

(Some figures in this article are in colour only in the electronic version)

1. Introduction

We investigate the dynamics of a spherical rigid body rolling on a plane. The distribution of
mass is non-uniform, so that the centre of mass does not coincide with the geometric centre.
However, the line joining the mass centre and geometric centre is assumed to be a principal
axis. We denote the principal moments of inertia by I_1, I_2 and I_3, and assume that $I_1 \leqslant I_2 < I_3$.
The symmetric case, when $I_1 = I_2$, was first studied by Routh [15], and in this case the body
is called Routh's sphere. There are three constants of motion and the system is integrable. In
the asymmetric case, $I_1 \neq I_2$, the system is no longer known to be integrable, and we find that
even a small degree of asymmetry (i.e. a small deviation of $\epsilon = (I_2 - I_1)/I_1$ from zero) has a
dramatic effect on the motion of the body.

Figure 1. The physical rock'n'roller constructed by slicing off a polar cap from a standard bowling ball. The polar angle is $\Theta \approx 53°$.

The equations of the symmetric loaded sphere are identical to those governing the motion of the tippe-top, which has been studied extensively (see [7] for a comprehensive reference list). However, in the case of the tippe-top, the angular momentum about the principal axis with maximum moment of inertia is large, and the sliding friction plays a key role. In the case under consideration here, we are interested in solutions where the angular velocity remains moderate and there is pure rolling contact. There are two characteristic modes of behaviour: pure rocking motion in a vertical plane, and pure circular rolling motion. The general motion has aspects of both these special cases, which leads us to name the body the *rock'n'roller*.

This investigation arose from the observation of the oscillations of a glass candle holder, spherical in form with an opening at the top. For a more systematic study, we constructed a larger and more massive body by removing a polar cap from a bowling ball to produce a truncated sphere (figure 1). As long as the tilting angle is such that the geometric centre is vertically above the contact point, the dynamics are equivalent to those of a loaded sphere. It was found that when the ball was tilted over to an angle of about 130°, it rocked back and forth but also precessed through an azimuthal angle that alternately increased and decreased. This unexpected and surprising *recession*[1], or reversal of precession, demanded an explanation in terms of dynamics.

We will show that for a symmetric loaded sphere reversal of the precession is impossible. This raises the question: what factor is missing from our dynamical model? We rule out sliding friction, since the motion is gentle with no evidence of slipping. Random perturbations, due to the imperfect shape of the ball or irregularities of the underlying surface, were not considered

---

[1] Note that the word *recession* is used here not as an antonym of precession, but with the meaning of 'reversal of action', as given, for example, in http://thesaurus.reference.com/.
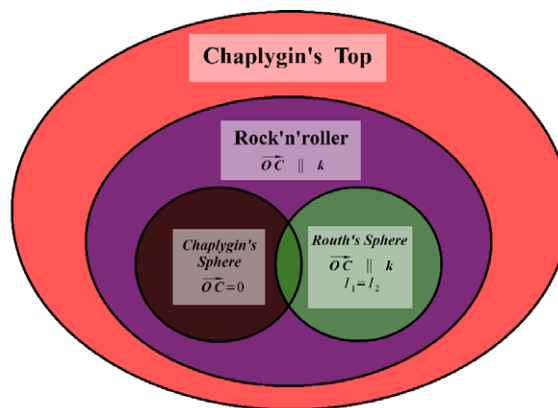
Figure 2. Hierarchy of loaded spheres. The vector $\overrightarrow{OC}$ is from the mass centre O to the geometric centre C, and $\mathbf{k}$ is the unit vector along the I_3-axis. See the text for details.

as a likely cause of the behaviour, as experiments indicated that the recession was quite a robust feature of the motion.

Although bowling balls are manufactured to high tolerance, and deviations from perfect sphericity must be very small, slight anomalies in the mass distribution are unavoidable. Moreover, the recesses in the physical body remaining from the finger holes introduce some asymmetry (figure 1). We were thus led to study the dynamics when the inertial symmetry $I_1 = I_2$ is broken. We find that even a minute deviation from symmetry changes the behaviour of the numerical solution profoundly. Of the three quantities conserved in the symmetric case (total energy E, Jellett's quantity Q_J and Routh's quantity Q_R), only the energy remains invariant when $I_1 \neq I_2$. We derive the equations governing the general motion and present analytical and numerical evidence of recession. We base our analysis on the existence of critical lines dividing the (Q_R, Q_J) plane into four dynamically disjoint zones. We prove that recession implies the lack of conservation of Jellett's and Routh's quantities, by identifying individual reversals as crossings of the orbit $(Q_R(t), Q_J(t))$ through the critical lines. This leads to a method of defining initial conditions for which the system will exhibit recession.

The rock'n'roller is one of a hierarchy of loaded spheres. For the most general case, the vector $\overrightarrow{OC}$ from the mass centre O to the geometric centre C does not lie on a principal axis, and all moments of inertia are distinct. This is called Chaplygin's top [3]. For the rock'n'roller, the geometric centre lies on a principal axis and $\overrightarrow{OC}$ is parallel to $\mathbf{k}$, the unit vector along the I_3-axis. Routh's sphere is the special case of this with $I_1 = I_2$ and Chaplygin's sphere the special case where the mass centre and geometric centre coincide. The hierarchy is illustrated in figure 2. For recent discussions, see [2, 4, 5, 9, 10, 16, 17]. Animations generated using numerical solutions of the equations for the rock'n'roller may be found at http://mathsci.ucd.ie/~plynch/RnR.

2. Symmetric body ($I_1 = I_2$): the dynamical equations

We consider a body, spherical in shape with unit mass and unit radius, whose mass distribution is non-uniform but symmetric about some line through the centre. We assume that the centre of mass is off-set a distance a from the geometric centre and that the moments of inertia perpendicular to and along the symmetry axis are I_1 and I_3, with $I_1(=I_2) < I_3$. All the
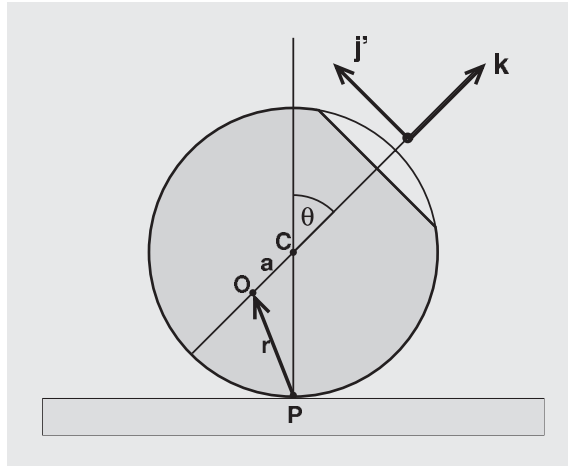
Figure 3. The intermediate coordinate frame used to study Routh's sphere.

parameters are determined once the angle of the polar cap that is removed is known (see appendix A.1). In an inertial frame of reference, the equations governing the dynamics of the body are

$$\frac{\mathrm{d}\boldsymbol{v}}{\mathrm{d}t} = \boldsymbol{F} \tag{1}$$

where $\boldsymbol{v}$ is the velocity of the centre of mass in the absolute frame and $\boldsymbol{F}$ is the total force acting on the body; and

$$\frac{\mathrm{d}\boldsymbol{L}}{\mathrm{d}t} = \boldsymbol{G} \tag{2}$$

where $\boldsymbol{L}$ is the intrinsic angular momentum and $\boldsymbol{G}$ is the total moment about the centre of mass.

The derivation in this section is similar to that in [19]. We consider a rotating frame of reference, with unit triad $(\boldsymbol{i}', \boldsymbol{j}', \boldsymbol{k}')$, whose origin moves with the centre of mass of the body. The vector $\boldsymbol{k}'$ is aligned with the axis of symmetry of the body and $\boldsymbol{j}'$ is aligned in the same vertical plane as $\boldsymbol{k}'$ (see figure 3). Then $\boldsymbol{i}'$ is horizontal and perpendicular to the plane shown in the figure, pointing inward. We use primes for this intermediate frame to distinguish it from the body frame that will be introduced in section 4 below.

The angular velocity of the body, expressed in the intermediate frame, is

$$\boldsymbol{\omega} = \omega_1' \boldsymbol{i}' + \omega_2' \boldsymbol{j}' + \omega_3' \boldsymbol{k}'.$$

Although this frame is not fixed in the body, it forms a set of principal axes in the symmetric case, $I_1 = I_2$, and the angular momentum is given by

$$\boldsymbol{L} = I_1 \omega_1' \boldsymbol{i}' + I_1 \omega_2' \boldsymbol{j}' + I_3 \omega_3' \boldsymbol{k}'.$$

We denote the angular velocity of the frame itself by $\boldsymbol{\Omega}$ and note that

$$\boldsymbol{\Omega} = \dot{\theta} \boldsymbol{i}' + \dot{\phi} \boldsymbol{K} = \dot{\theta} \boldsymbol{i}' + s\dot{\phi} \boldsymbol{j}' + c\dot{\phi} \boldsymbol{k}' = (\Omega_1, \Omega_2, \Omega_3) \tag{3}$$

where $s = \sin\theta$, $c = \cos\theta$ and $\boldsymbol{K}$ is a unit vertical vector. The Euler angles (θ, ϕ, ψ) are related to the components of angular velocity by

$$\omega_1' = \dot{\theta}, \qquad \omega_2' = s\dot{\phi}, \qquad \omega_3' = c\dot{\phi} + \dot{\psi}. \tag{4}$$

Definitions are standard, and may be found in [12, 18, 20]. For a list of the principal symbols used in this study, see table 1.

4

Table 1. Principal symbols used in this study.

Symbol	Meaning
F	Total forcing in Newton's equation
G	Total moment in Newton's equation
I_1, I_2, I_3	Principal moments of inertia of body
K	Unit vertical vector
L	Angular momentum of a body about centre of mass
$\mathcal{L}$	Lagrangian function
Q_J	Jellett's quantity, constant in the symmetric case
Q_R	Routh's quantity, constant in the symmetric case
R	Force of reaction at a contact point
T	Total kinetic energy
V	Potential energy
V	Velocity of centre of mass in the space frame
W	Force due to gravity (weight)
a	Distance from the geometric centre to the centre of mass
c	Cosine of tilting angle, $c = \cos\theta$
c_ϕ	Cosine of azimuthal angle, $c_\phi = \cos\phi$
d	Cosine of polar angle, $d = \cos\Theta$
f	Projection of vertical radius on the k-axis, $f = \cos\theta - a$
g	Acceleration of gravity
h	Height of centre of mass, $h = 1 - a\cos\theta$
i, j, k	Principal unit orthogonal triad in body coordinates
i', j', k'	Principal unit orthogonal triad in body coordinates
r	Moment vector, from the contact point to the mass centre
s	Sine of tilting angle, $s = \sin\theta$
s_ϕ	Sine of azimuthal angle, $s_\phi = \sin\phi$
t	Time
v	Velocity of centre of mass in the body frame
v_1, v_2, v_3	Components of v in body coordinates
Θ	Co-latitude of a polar cap removed to construct the rock'n'roller.
Υ	Rotation matrix
Φ	Azimuthal angle spanned by the solution, $\Phi = \phi_{\max} - \phi_{\min}$
Ω	Angular velocity of the intermediate frame
ϵ	Asymmetry parameter, $\epsilon = (I_2 - I_1)/I_1$
θ, ϕ, ψ	Euler angles (tilting, azimuth and spinning angles)
μ_k	Lagrange multipliers
ρ	Measure quantity, $\rho = [I_3 + s^2 + (I_3/I_1)f^2]^{-1/2}$
σ	Sine of spining angle, $\sigma = \sin\psi$
τ	Period of rocking motion
χ	Cosine of spinning angle, $\chi = \cos\psi$
ω	Angular velocity of a body
$\omega_1', \omega_2', \omega_3'$	Components of ω in intermediate coordinates
$\omega_1, \omega_2, \omega_3$	Components of ω in body coordinates

2.1. Equations in the intermediate frame

In the moving frame, equations (1) and (2) become respectively

$$\frac{d\boldsymbol{v}}{dt} + \boldsymbol{\Omega} \times \boldsymbol{v} = \boldsymbol{F} \tag{5}$$

and

$$\frac{d\boldsymbol{L}}{dt} + \boldsymbol{\Omega} \times \boldsymbol{L} = \boldsymbol{G}. \tag{6}$$

Expanding these in components in the $\boldsymbol{i}'\boldsymbol{j}'\boldsymbol{k}'$-frame, we get

$$\begin{aligned}
\dot{v}'_1 + \Omega_2 v'_3 - \Omega_3 v'_2 &= F_1 \\
\dot{v}'_2 + \Omega_3 v'_1 - \Omega_1 v'_3 &= F_2 \\
\dot{v}'_3 + \Omega_1 v'_2 - \Omega_2 v'_1 &= F_3
\end{aligned} \tag{7}$$

for momentum. The angular momentum equations become

$$\begin{aligned}
I_1 \dot{\omega}'_1 + I_3 \Omega_2 \omega'_3 - I_1 \Omega_3 \omega'_2 &= G_1 \\
I_2 \dot{\omega}'_2 + I_1 \Omega_3 \omega'_1 - I_3 \Omega_1 \omega'_3 &= G_2 \\
I_3 \dot{\omega}'_3 &= G_3.
\end{aligned} \tag{8}$$

Equations (7) and (8) are identical to (12.412) in [18] (with $I_1 = I_2$).

The forces acting on the body are gravity $\boldsymbol{W} = (0, -gs, -gc)$ and the force of reaction $\boldsymbol{R} = (R_1, R_2, R_3)$:

$$\boldsymbol{F} = \boldsymbol{W} + \boldsymbol{R}.$$

Defining $f = c - a$, the vector from the point of contact P to the centre of mass O is $\boldsymbol{r} = (0, s, f)$ (see figure 3). Then the total moment about O is given by $\boldsymbol{G} = -\boldsymbol{r} \times \boldsymbol{R}$. The *constraint of no slipping* at the contact point requires that the body is instantaneously rotating about this point. Thus,

$$\boldsymbol{v} = \boldsymbol{\omega} \times \boldsymbol{r} = (f\omega'_2 - s\omega'_3, -f\omega'_1, s\omega'_1). \tag{9}$$

The reactive forces may be eliminated by combining the angular momentum equation (6) with the vector product of $\boldsymbol{r}$ and the momentum equation (5). The velocity $\boldsymbol{v}$ may be expressed in terms of the rotation $\boldsymbol{\omega}$ by means of the constraint (9). We then obtain three equations for ω_1, ω_2 and ω_3:

$$\begin{bmatrix} I_1 + s^2 + f^2 & 0 & 0 \\ 0 & I_1 + f^2 & -fs \\ 0 & -fs & I_3 + s^2 \end{bmatrix} \begin{pmatrix} \dot{\omega}'_1 \\ \dot{\omega}'_2 \\ \dot{\omega}'_3 \end{pmatrix} = \begin{pmatrix} P_1 \\ P_2 \\ P_3 \end{pmatrix} \tag{10}$$

where P_1, P_2 and P_3 depend on the angles and angular velocities. Full details of the derivation are presented in appendix (A.2). The rates of change of the angular variables follow from (4):

$$\dot{\theta} = \omega'_1, \qquad \dot{\phi} = \omega'_2/s, \qquad \dot{\psi} = \omega'_3 - (c/s)\omega'_2. \tag{11}$$

We now have six equations (10) and (11) for the six variables $\{\theta, \phi, \psi, \omega'_1, \omega'_2, \omega'_3\}$.

2.2. Special solutions

2.2.1. Pure rocking. For pure rocking motion, with no change of azimuthal angle and no rotation about the axis of symmetry, we have $\phi = \psi = 0$ and so $\omega'_2 = \omega'_3 = 0$. Then the system reduces to a single equation for the tilting angle θ:

$$\ddot{\theta} + \left[\frac{(g + \dot{\theta}^2)a}{I_1 + f^2 + s^2} \right] \sin\theta = 0. \tag{12}$$

For small amplitude $\theta \ll 1$, and assuming $a \ll 1$, this becomes

$$\ddot{\theta} + \left[\frac{ga}{I_1 + 1} \right] \theta = 0, \tag{13}$$

the equation for simple harmonic oscillations.

2.2.2. Pure rolling.

For the case of pure circular rolling motion we have

$$\dot{\theta} = 0, \qquad \dot{\phi} = \text{constant}, \qquad \dot{\psi} = \text{constant}$$

so that $\Omega_1 = \omega_1' = 0$ and ω_2' and ω_3' are constants. It follows immediately that $P_2 = P_3 = 0$ (see (A.2)). The requirement that $\theta = \theta_0$, constant, implies $P_1 = 0$, which yields a relationship between ω_2' and ω_3':

$$\omega_3' = \frac{(I_1 \cot \theta_0 + m h_0 f_0 \csc \theta_0)\omega_2'^2 - ga \sin \theta_0}{(I_3 + h_0)\omega_2'} \tag{14}$$

where $f_0 = \cos \theta_0 - a$ and $h_0 = 1 - a \cos \theta_0$ are constants. If we start with ω_2' and ω_3' related by (14) and θ slightly perturbed from θ_0, motion with nutation about θ_0 results.

2.3. Constants of motion and general solution

We consider the case of a perfectly rough contact, with rolling motion. Given that there are two symmetries in the problem, invariance under addition of arbitrary constants to either ϕ or ψ, we might expect two invariants in addition to the total energy. For general initial conditions, there are three constants of integration. They are the total energy, Jellett's constant and Routh's constant (see [7] for a complete derivation of these constants).

The kinetic energy is the sum of translational and rotational components:

$$T = \tfrac{1}{2}\left[v_1'^2 + v_2'^2 + v_3'^2 \right] + \tfrac{1}{2}\left[I_1 \omega_1'^2 + I_2 \omega_2'^2 + I_3 \omega_3'^2 \right]$$

and the potential energy is

$$V = ga(1 - \cos \theta).$$

Then, since there is no dissipation, the total energy

$$E = T + V \tag{15}$$

is conserved. Jellett's constant is the scalar product of the angular momentum and the vector joining the point of contact to the centre of mass:

$$Q_J = \boldsymbol{L} \cdot \boldsymbol{r} = I_1 s \, \omega_2' + I_3 f \, \omega_3', \tag{16}$$

and Routh's constant, more difficult to interpret physically, is

$$Q_R = \frac{\omega_3'}{\rho} \tag{17}$$

where, following [2], we define the measure

$$\rho(\theta) = 1/\sqrt{I_3 + s^2 + (I_3/I_1) f^2}. \tag{18}$$

Note that our definition of Routh's constant differs from the usual quadratic function of ω_3', in [15], [7] and elsewhere.

An interesting historical discussion of these constants may be found in [7]. Note that the constancy of Q_R implies conservation of the *sign* of ω_3': since the measure ρ is positive definite, ω_3' cannot pass through zero. For the tippe-top, this precludes the tipping phenomenon for the case of rolling motion.

From equations (11) determining the rates of change of the angles, we can solve explicitly for $\dot{\phi}$ and $\dot{\psi}$ in terms of θ and Jellett's and Routh's constants:

$$\dot{\phi} = V_\phi(\theta, Q_R, Q_J) \equiv \frac{1}{I_1 s^2}[Q_J - \rho f I_3 Q_R], \tag{19}$$

$$\dot{\psi} = V_\psi(\theta, Q_R, Q_J) \equiv -\frac{1}{I_1 s^2}[c Q_J - \rho(c f I_3 + I_1 s^2) Q_R]. \tag{20}$$

Since Q_J and Q_R are constants, the rates of change $\dot{\phi}$ and $\dot{\psi}$ are determined as single-valued functions of the angle θ. We will show in the next section that recession, or reversal of precession, implies in particular that $\dot{\phi}$ and $\dot{\psi}$ at a given angle θ systematically change their sign as time evolves. Therefore, in the symmetric case it is impossible to have recession for Routh's Sphere.

We can use the constants of motion to reduce the system to a single equation for the tilting angle θ. We use Routh's constant (17) to obtain $\omega'_3(\theta)$. Then Jellett's constant (16) gives $\omega'_2(\theta)$. Finally, the energy (15) gives an expression for $\omega'_1(\theta)$, yielding an equation of the form

$$\dot{\theta}^2 = F(\theta), \tag{21}$$

which may be integrated to obtain $\theta(t)$. As a result, the system can be explicitly integrated. However, we will not derive explicit analytical expressions for $F(\theta)$ and $\theta(t)$. The reader is referred to [7] for a more explicit treatment; see also [4, 16]. We see that the evolution of $\theta(t)$ obtained from (21) gives the rocking component of the motion, while the evolution of $\phi(t)$ and $\psi(t)$, obtained from (19) and (20), gives the rolling and spinning components of the motion respectively.

2.4. Precession of the rocking motion

The generic motion of the symmetric body is quasi-periodic. On the one hand there is a period τ of the rocking motion, determined by the equation

$$\tau = 4 \int_{\theta_N}^{\theta_X} \frac{\mathrm{d}\theta}{\sqrt{F(\theta)}},$$

where $0 \leqslant \theta_N \leqslant \theta_X \leqslant \pi$, and θ_N and θ_X are the *turning points* where $F(\theta_N) = 0$ and $F(\theta_X) = 0$. On the other hand, the rolling motion during this period can be computed by integrating the rates of change of the angles ϕ and ψ from (19) and (20) respectively:

$$\Delta\phi = \int_0^\tau V_\phi(\theta(t), Q_R, Q_J)\,\mathrm{d}t = 4 \int_{\theta_N}^{\theta_X} \frac{V_\phi(\theta, Q_R, Q_J)}{\sqrt{F(\theta)}}\,\mathrm{d}\theta, \tag{22}$$

with an analogous formula for the angle $\Delta\psi$. Generically, $\Delta\phi$ is not commensurate with 2π; this implies the quasi-periodicity of the precessing motion. As a consequence of quasi-periodicity, the projection of the trajectory onto the θ–ϕ plane densely covers a two-dimensional region.

In order to quantify the precession, we distinguish two angles, the *full azimuthal angle* ϕ and the *visible angle* $\phi \,(\mathrm{mod}\,2\pi)$, which is the angle that is seen by an observer in the space frame. (We will occasionally use the *visible half-angle* $\phi \,(\mathrm{mod}\,\pi)$, which gives more illustrative plots in the case of the (asymmetric) rock'n'roller.) Correspondingly, there will be two types of precession angle: $\Delta\phi$, the *full precession angle* defined by (22), and $\Delta\phi \,(\mathrm{mod}\,2\pi)$, the *visible precession angle*.

2.5. Qualitative analysis of the precession. Criticality

We now estimate the precession angles $\Delta\phi$ and $\Delta\phi \pmod{2\pi}$ from (22). Heuristically, the main contribution comes from the regions near the turning points, where $F(\theta) = 0$. The relative contributions at θ_N and θ_X will be determined by the magnitude and sign of $V_\phi(\theta, Q_R, Q_J)$ at the turning points. It is therefore useful to study separately the behaviour of $V_\phi(\theta, Q_R, Q_J)$ for θ in each of the asymptotic regions $\theta \approx 0$ and $\theta \approx \pi$.

- Asymptotic region $\theta \approx 0$. A Laurent expansion of (19) gives

$$V_\phi(\theta, Q_R, Q_J)|_{\theta \approx 0} = \frac{1}{I_1 \theta^2} \left(Q_J - Q_{J,0}^{\mathrm{crit}} \right) + \mathcal{O}(1), \tag{23}$$

where we define the 'critical Jellett quantity at $\theta = 0$' as

$$Q_{J,0}^{\mathrm{crit}} \equiv \rho_0 (1-a) I_3 Q_R, \tag{24}$$

with $\rho_0 = 1/\sqrt{I_3 + (I_3/I_1)(1-a)^2}$.

- Asymptotic region $\theta \approx \pi$. A Laurent expansion of (19) gives

$$V_\phi(\theta, Q_R, Q_J)|_{\theta \approx \pi} = \frac{1}{I_1 (\pi - \theta)^2} \left(Q_J - Q_{J,\pi}^{\mathrm{crit}} \right) + \mathcal{O}(1), \tag{25}$$

where we define the 'critical Jellett quantity at $\theta = \pi$' as

$$Q_{J,\pi}^{\mathrm{crit}} \equiv -\rho_\pi (1+a) I_3 Q_R, \tag{26}$$

with $\rho_\pi = 1/\sqrt{I_3 + (I_3/I_1)(1+a)^2}$.

- Monotonicity property. The factor $[Q_J - \rho f I_3 Q_R]$ appearing on the right-hand side of (19) is a monotonic function of the angle $\theta \in [0, \pi]$. The proof of this is straightforward.

From the above asymptotic expansions, we conclude that, in the space of initial conditions parameterized by (Q_R, Q_J), there are four regions of interest, and the behaviour of $\dot{\phi}$ is qualitatively different in each region.

Region I: $Q_R > 0$, $Q_{J,\pi}^{\mathrm{crit}} < Q_J < Q_{J,0}^{\mathrm{crit}}$. The function $V_\phi(\theta, Q_R, Q_J)$ goes from $-\infty$ at $\theta = 0$ to ∞ at $\theta = \pi$. From the monotonicity property it follows that this function has a single zero.

Region II: $Q_{J,\pi}^{\mathrm{crit}} < Q_J$, $Q_{J,0}^{\mathrm{crit}} < Q_J$. The function $V_\phi(\theta, Q_R, Q_J)$ goes from ∞ at $\theta = 0$ to ∞ at $\theta = \pi$. From the monotonicity property it is possible to show that this function is positive definite and has a single minimum.

Region III: $Q_R < 0$, $Q_{J,0}^{\mathrm{crit}} < Q_J < Q_{J,\pi}^{\mathrm{crit}}$. The function $V_\phi(\theta, Q_R, Q_J)$ goes from ∞ at $\theta = 0$ to $-\infty$ at $\theta = \pi$. From the monotonicity property it follows that this function has a single zero.

Region IV: $Q_J < Q_{J,\pi}^{\mathrm{crit}}$, $Q_J < Q_{J,0}^{\mathrm{crit}}$. The function $V_\phi(\theta, Q_R, Q_J)$ goes from $-\infty$ at $\theta = 0$ to $-\infty$ at $\theta = \pi$. From the monotonicity property it is possible to show that this function is negative definite and has a single maximum.

Similar results can be obtained for the velocities $\dot{\psi}$, but these are omitted here.

In figure 4 we show the four regions separated by the two critical lines $Q_J = Q_{J,\pi}^{\mathrm{crit}}$ (line from top left to bottom right) and $Q_J = Q_{J,0}^{\mathrm{crit}}$ (line from bottom left to top right). Typical plots of the function $V_\phi(\theta, Q_R, Q_J)$ versus θ are inserted in each region. The asymptotic behaviours are evident.

The critical Jellett quantity $Q_{J,\pi}^{\mathrm{crit}}$ plays a key role in determining the visible precession angle $\Delta\phi \pmod{2\pi}$ in the interesting case $\theta_X \approx \pi$. The main contribution to the precession angle comes from the turning point $\theta = \theta_X$ and from (25); we see that the sign of this contribution depends on the sign of $Q_J - Q_{J,\pi}^{\mathrm{crit}}$. For example, if an initial condition with
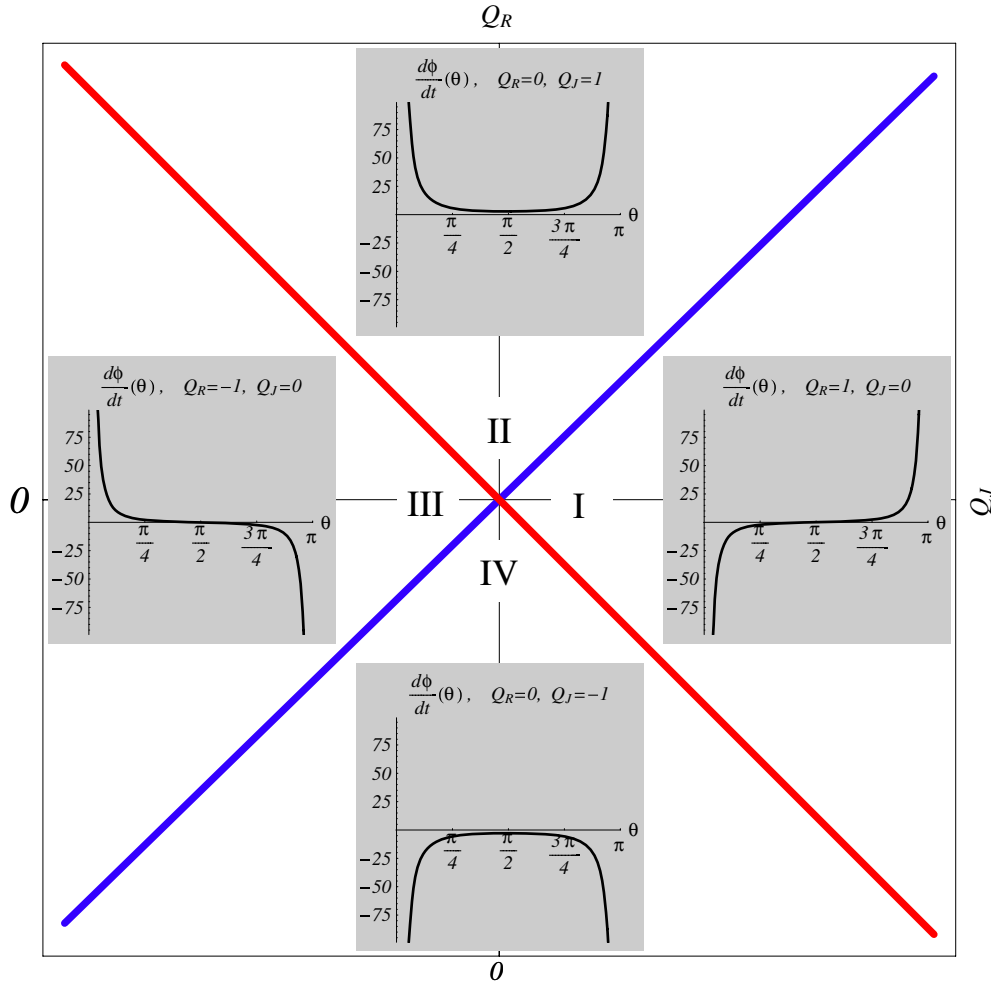
Figure 4. The four critical regions defined by the critical lines $Q_J = Q_{J,\pi}^{\mathrm{crit}}$ (red online, top left to bottom right) and $Q_J = Q_{J,0}^{\mathrm{crit}}$ (blue online, bottom left to top right). In each region, the graph of $\dot{\phi}$ as a function of θ is shown, for the selected values Q_R, Q_J and parameters $a = 0.05$, $I_3 = 2/5$ and $I_1 = (1 - 5\,a/2)I_3$.

$Q_J - Q_{J,\pi}^{\mathrm{crit}} \gtrless 0$ (regions I or II) has a precession angle $\Delta\phi = \alpha_0 \pmod{2\pi}$, then a slightly different initial condition with $Q_J - Q_{J,\pi}^{\mathrm{crit}} \lessgtr 0$ (region IV or III) will have a precession angle $\Delta\phi = -\alpha_0 \pmod{2\pi}$; the corresponding motion will appear to be reversed.

   The critical Jellett quantity $Q_{J,0}^{\mathrm{crit}}$ determines the full precession angle $\Delta\phi$ when $\theta_N \approx 0$. The main contribution to $\Delta\phi$ comes from the turning point θ_N, and is given by rapid changes of ϕ in jumps of approximately $\pm\pi$, the sign of these jumps depending on the sign of $Q_J - Q_{J,0}^{\mathrm{crit}}$. In this way, an initial condition in region I or IV will give rise to a full-angle precession $\Delta\phi < 0$, whereas for initial conditions in region II or III, $\Delta\phi > 0$. It is worth mentioning that this critical quantity is related to the energy of the system since it appears in the Laurent expansion of the function $F(\theta)$ near $\theta = 0$. See [7], where this critical quantity was identified in terms of the centrifugal barrier.

2.6. Quantitative estimate of applicability of criticality criteria

Let us consider the asymptotic region $\theta \approx \pi$. For the above asymptotic analysis to be of practical importance, the maximum rocking angle θ_X must be close to π. Only then will the asymptotic Laurent expansion (25) determine, to a good approximation, the value of $\dot{\phi}$ at $\theta = \theta_X$. In particular, we will observe a dramatic difference in $\dot{\phi}$ at $\theta = \theta_X$ and in the precession angle when considering two nearby points, one in region I and the other in region IV.

To quantify how close should θ_X be to π, *necessary* conditions are (i) in regions I and III, θ_z, the zero of $\dot{\phi}(\theta)$ must be less than θ_X; (ii) In regions II and IV, θ_e, the extremum of $\dot{\phi}(\theta)$ must be less than θ_X. In each case, there is a relation between θ_X, Q_R, Q_J and the parameters a, I_1, I_3 respectively.

For regions I and III, this condition has a simple analytical formulation:

$$-1 \leqslant \cos\theta_X \leqslant \cos\theta_z \equiv \frac{a\beta I_3 + \sqrt{I_1(I_3 - \beta)[\beta(I_3 - I_1)(I_3 + 1) - a^2\beta I_3 + I_1 I_3(I_3 + 1)]}}{\beta(I_3 - I_1) + I_1 I_3}$$

where $\beta = I_3 - (Q_J/Q_R)^2$. Realistic values of parameters and ratio Q_J/Q_R allow any value of θ_X in the interval $(0, \pi)$.

It is noteworthy that, near the critical line $Q_J = Q_{J,\pi}^{\mathrm{crit}}$, the necessary condition is satisfied if and only if $\theta_X \approx \pi$. Letting $Q_J / Q_{J,\pi}^{\mathrm{crit}} = 1 - \delta$ we get

$$\pi \geqslant \theta_X \geqslant \pi - \left(\sqrt{\frac{2(1 + a)[(1 + a)^2 + I_1]I_3}{I_1(I_3 + 1 + a)}}\right)\delta^{1/2} + O(\delta^{3/2}). \tag{27}$$

3. Recession of the asymmetric body ($I_1 \neq I_2$)

In this section we give a precise description of recession, or reversal of precession, of the rock'n'roller. The definition is based on observational evidence: for initial conditions close to pure rocking motion and such that the local maxima (turning points) of the tilting angle θ are in the range $(\sim 3/4\pi, \pi)$, the rates of change $\dot{\phi}(t_j)$ and $\dot{\psi}(t_j)$ at times t_j, $j = 1, \ldots, \infty$, where the angle $\theta(t_j)$ is a (local) maximum $\theta_X(t_j)$, depend on the time t_j, contrary to the case of the symmetric body. The functions $\dot{\phi}(t_j)$ and $\dot{\psi}(t_j)$ have a quasi-periodic behaviour, undergoing changes of sign that translates observationally to alternating reversals of the visible precession angles $\Delta\phi(t_j) \pmod{2\pi}$ and $\Delta\psi(t_j) \pmod{2\pi}$, where

$$\Delta\phi(t_j) = \int_{t_{j-2}}^{t_j} \dot{\phi}(t)\,\mathrm{d}t, \qquad \Delta\psi(t_j) = \int_{t_{j-2}}^{t_j} \dot{\psi}(t)\,\mathrm{d}t.$$

Note that the integration is from t_{j-2} to t_j, which accounts for a full period of motion. In the dynamical region of interest, $\theta_X(t_j) \in (\sim 3/4\pi, \pi)$, the critical quantities defined in section 2.5 allow us to understand the behaviour qualitatively, and to predict the occurrence of reversals.

The key observation from numerical simulations is that, in the asymmetric case, the Jellett and Routh quantities, (16) and (17), cease to be conserved, but *oscillate* about mean values. We thus *define* the Jellett and Routh quantities Q_J and Q_R respectively to be

$$Q_J(t) = I_1 s\omega_2' + I_3 f\omega_3', \qquad Q_R(t) = \frac{\omega_3'}{\rho}. \tag{28}$$

We have observed that these quantities oscillate about time-averaged values with a period that is generally longer than the period of the rocking motion, and that depends on the amplitude of the motion. We remark that the motion in the (Q_R, Q_J)-plane is bounded. We will perform

a numerical study of this behaviour in connection with reversals at the end of the next section. The analytical study of this will be the subject of forthcoming work.

The analysis in section 2.5 regarding the asymptotic behaviour of $\dot{\phi}$ near the turning points remains valid if we consider $Q_J(t)$ and $Q_R(t)$ to be functions of time. In particular, as long as the point $(Q_R(t), Q_J(t))$ remains within one of the regions I–IV, we can safely conclude that there is no reversal of the system, because the sign of $\dot{\phi}$ at the turning points cannot possibly change. Reversal is due to crossing of the system from one region to an adjacent one. In order to observe reversal, we need to initialize the system sufficiently close to the boundary of a region in such a way that, during the evolution of the motion, the system crosses the boundary. We call this a *critical crossing*. Due to the oscillating nature of $Q_J(t)$ and $Q_R(t)$ evidenced in numerical simulations, if this critical crossing happens, then the system will eventually cross back to the original region and will continue crossing periodically back and forth between the two regions, in a bounded motion within the space (Q_R, Q_J).

Corresponding to the critical crossings of the two types of critical quantities—$Q_{J,0}^{\text{crit}}$ defined at the turning point near $\theta = 0$ and $Q_{J,\pi}^{\text{crit}}$ defined at that near $\theta = \pi$—there are two types of reversal. On the one hand, the *full angle*, $\phi(t)$, has reversals that are related to the critical crossings of $Q_{J,0}^{\text{crit}}$. This is due to the fact that, for motion close to pure rocking, the main change of $\phi(t)$ from $t = t_{j-1}$ to $t = t_j$ is typically a jump of magnitude about π when θ passes the turning point θ_N. The sign of this jump depends on which critical region the system is in, and will therefore change when reversal occurs. Critical crossings from region I to region II or from region III to region IV correspond to this type of reversal.

On the other hand, the *visible precession angle*, $\Delta\phi(t_j) \,(\text{mod}\, 2\pi)$, is mainly due to the change of $\phi(t)$ near the turning point θ_X. The sign of this change depends exclusively on the criticality $Q_{J,\pi}^{\text{crit}}$. Critical crossings from region IV to region I or from region II to region III determine this type of reversal. This reversal corresponds to the recession evident in real experiments. A numerical study of the two types of reversal will be presented in section 6 below.

4. Asymmetric body ($I_1 \neq I_2$): the dynamical equations

We now derive the equations for the asymmetric case $I_1 \neq I_2$. Since the intermediate frame (i', j', k') is no longer a principal frame, it is convenient to use a body frame (i, j, k) aligned in the direction of the principal axes. The angular velocity and angular momentum are then respectively

$$\boldsymbol{\omega} = \omega_1 \boldsymbol{i} + \omega_2 \boldsymbol{j} + \omega_3 \boldsymbol{k} \qquad \boldsymbol{L} = I_1 \omega_1 \boldsymbol{i} + I_2 \omega_2 \boldsymbol{j} + I_3 \omega_3 \boldsymbol{k}.$$

The momentum equations of motion in the body frame are

$$\begin{aligned}
\dot{v}_1 + \omega_2 v_3 - \omega_3 v_2 &= F_1 \\
\dot{v}_2 + \omega_3 v_1 - \omega_1 v_3 &= F_2 \\
\dot{v}_3 + \omega_1 v_2 - \omega_2 v_1 &= F_3
\end{aligned} \tag{29}$$

and the angular momentum equations are

$$\begin{aligned}
I_1 \dot{\omega}_1 + (I_3 - I_2)\omega_2 \omega_3 &= G_1 \\
I_2 \dot{\omega}_2 + (I_1 - I_3)\omega_3 \omega_1 &= G_2 \\
I_3 \dot{\omega}_3 + (I_2 - I_1)\omega_1 \omega_2 &= G_3.
\end{aligned} \tag{30}$$

We proceed as in section 2, using constraint (9), to express the velocity v in terms of the rotation ω and eliminating the moment G by means of the momentum equations. The result may be written as

$$\Sigma\dot{\theta} = \omega, \qquad K\dot{\omega} = P_\omega \tag{31}$$

where

$$\dot{\theta} = \begin{pmatrix} \dot{\theta} \\ \dot{\phi} \\ \dot{\psi} \end{pmatrix}, \qquad \dot{\omega} = \begin{pmatrix} \dot{\omega}_1 \\ \dot{\omega}_2 \\ \dot{\omega}_3 \end{pmatrix},$$

the matrices Σ and K are respectively

$$\Sigma = \begin{bmatrix} \chi & s\sigma & 0 \\ -\sigma & s\chi & 0 \\ 0 & c & 1 \end{bmatrix} \qquad K = \begin{bmatrix} I_1 + f^2 + s^2\chi^2 & -s^2\sigma\chi & -fs\sigma \\ -s^2\sigma\chi & I_2 + f^2 + s^2\sigma^2 & -fs\chi \\ -fs\sigma & -fs\chi & I_3 + s^2 \end{bmatrix}, \tag{32}$$

and the vector P_ω is

$$P_\omega = \begin{pmatrix} -(g + \omega_1^2 + \omega_2^2)as\chi + (I_2 - I_3 - af)\omega_2\omega_3 \\ (g + \omega_1^2 + \omega_2^2)as\sigma + (I_3 - I_1 + af)\omega_1\omega_3 \\ (I_1 - I_2)\omega_1\omega_2 + as(-\chi\omega_1 + \sigma\omega_2)\omega_3 \end{pmatrix},$$

with $\chi = \cos\psi$ and $\sigma = \sin\psi$. Note that neither K nor P_ω depends explicitly on ϕ. Thus, ϕ is an ignorable coordinate in the system (31).

4.1. Special solutions

We consider pure rocking motion with ϕ and ψ constants. Then $\omega = (\chi\dot{\theta}, -\sigma\dot{\theta}, 0)$. The system (31) implies

$$(I_1 - I_2)\sigma\chi\dot{\theta}^2 = 0$$

so that a nontrivial solution requires $\sigma\chi = 0$. That is, the rocking motion must be about one of the principal axes. For $\sigma = 0$ the system reduces to (12), pure rocking about the i-axis. For $\chi = 0$ we get the corresponding equation with I_2 replacing I_1 and pure rocking about the j-axis. From (13), the ratio of the small amplitude oscillations about these principal axes is

$$\frac{\nu_1}{\nu_2} = \sqrt{\frac{I_2 + 1}{I_1 + 1}}.$$

In general, there are no periodic solutions corresponding to the pure rolling motion found in the symmetric case. However, if θ remains zero, we may have spinning about the k-axis, with k vertical. Then $\omega = (0, 0, \dot{\psi})$. Equations (31) reduce to $I_3\dot{\omega}_3 = 0$, confirming that the spin rate is an arbitrary constant.

4.2. Nonholonomic constraints

The rock'n'roller is subject to three constraints, one holonomic and two nonholonomic. The body must remain in contact with the underlying surface, and the point of contact must be momentarily stationary to ensure rolling contact. We can embrace the three constraints in the single equation (9), i.e. $v = \omega \times r$. We will now express this in terms of the space frame. The velocities in the body and space frames, v and V respectively, are related by $v = \Upsilon^{\mathrm{T}}V$ or, explicitly,

$$\begin{pmatrix} v_1 \\ v_2 \\ v_3 \end{pmatrix} = \begin{bmatrix} c_\phi\chi - cs_\phi\sigma & -c_\phi\sigma - cs_\phi\chi & ss_\phi \\ s_\phi\chi + cc_\phi\sigma & -s_\phi\sigma + cc_\phi\chi & -sc_\phi \\ s\sigma & s\chi & c \end{bmatrix}^{\mathrm{T}} \begin{pmatrix} V_1 \\ V_2 \\ V_3 \end{pmatrix} \tag{33}$$

13

where $c_\phi = \cos\phi$ and $s_\phi = \sin\phi$. The matrix $\mathbf{\Upsilon}$ is the product of three rotations, and is derived in many standard texts in mechanics; see, for example, [8, 11, 12, 18, 20]. We write $\boldsymbol{\omega} \times \boldsymbol{r} = \mathbf{\Gamma}\boldsymbol{\omega}$ and $\boldsymbol{\omega} = \mathbf{\Sigma}\dot{\boldsymbol{\theta}}$, where

$$\mathbf{\Gamma} = \begin{bmatrix} 0 & f & -s\chi \\ -f & 0 & s\sigma \\ s\chi & -s\sigma & 0 \end{bmatrix}. \tag{34}$$

Now the constraints can be expressed in the form $V = \mathbf{\Upsilon}\mathbf{\Gamma}\mathbf{\Sigma}\dot{\boldsymbol{\theta}}$, relating the velocity in the space frame to the time derivatives of the Euler angles. More explicitly,

$$\begin{pmatrix} \dot{X} \\ \dot{Y} \\ \dot{Z} \end{pmatrix} = \begin{bmatrix} hs_\phi & -asc_\phi & -sc_\phi \\ -hc_\phi & -ass_\phi & -ss_\phi \\ as & 0 & 0 \end{bmatrix} \begin{pmatrix} \dot{\theta} \\ \dot{\phi} \\ \dot{\psi} \end{pmatrix}. \tag{35}$$

It is clear from this form that the constraint on $\dot{Z}$ is holonomic and may be integrated immediately to give $Z = 1 - ac = h$, the height of the mass centre in terms of the tilting angle θ. The constraints on $\dot{X}$ and $\dot{Y}$ are nonholonomic.

5. Lagrangian formulation

Systems with holonomic constraints can be solved by elimination of redundant coordinates or by adding to the Lagrangian a sum of the constraints weighted by Lagrange multipliers. When the constraints are nonholonomic, this procedure does not apply [11, 20]. We must resist the temptation to substitute (9) into the Lagrangian and obtain a Lagrangian that involves only the Euler angles and their derivatives. Rather, we must embed the problem in a configuration space of dimension $N+M$, where N is the number of degrees of freedom and M is the number of nonholonomic constraints. There has been considerable misunderstanding regarding nonholonomic constraints; see [6] for a review. When the constraints are of the form

$$g_k(\boldsymbol{q}, \dot{\boldsymbol{q}}, t) \equiv A_k(\boldsymbol{q}, t)\dot{\boldsymbol{q}} = 0,$$

that is, where they are linear in the velocities, we can write the equations of motion in the form

$$\frac{\mathrm{d}}{\mathrm{d}t}\frac{\partial\mathcal{L}}{\partial\dot{\boldsymbol{q}}} - \frac{\partial\mathcal{L}}{\partial\boldsymbol{q}} + \sum_k \mu_k \frac{\partial g_k}{\partial\dot{\boldsymbol{q}}} = 0, \tag{36}$$

where μ_k are Lagrange multipliers that can be determined using the constraints. In the present case, the configuration space has five dimensions, with coordinates $(\theta, \phi, \psi, X, Y)$, the holonomic constraint having been used to eliminate Z. We may write the Lagrangian in terms of these coordinates and their time derivatives:

$$\mathcal{L} = \tfrac{1}{2}\{(I_1\chi^2 + I_2\sigma^2 + a^2 s^2)\dot{\theta}^2 + 2(I_1 - I_2)s\chi\sigma\,\dot{\theta}\dot{\phi} + [(I_1\sigma^2 + I_2\chi^2)s^2 + I_3 c^2]\dot{\phi}^2$$
$$+ 2I_3 c\,\dot{\phi}\dot{\psi} + I_3\,\dot{\psi}^2 + (\dot{X}^2 + \dot{Y}^2)\} - ga(1 - c). \tag{37}$$

Note that $\mathcal{L}$ does not depend on ϕ. From (35), the nonholonomic constraints are

$$g_1 \equiv \dot{X} - (hs_\phi\,\dot{\theta} - asc_\phi\,\dot{\phi} - sc_\phi\,\dot{\psi}) = 0$$
$$g_2 \equiv \dot{Y} - (-hc_\phi\,\dot{\theta} - ass_\phi\,\dot{\phi} - ss_\phi\,\dot{\psi}) = 0. \tag{38}$$

Although ϕ occurs in these expressions, it is absent from the combinations $\sum_k \mu_k \partial g_k/\partial\dot{\boldsymbol{q}}$ that occur in the equations. This symmetry should imply the existence of an invariant quantity in addition to the total energy.

The Euler–Lagrange equations (36) for X and Y immediately yield respectively

$$\mu_1 = -\ddot{X} \qquad \mu_2 = -\ddot{Y}.$$

Using the constraints, we may now eliminate the multipliers μ_1 and μ_2 from the remaining equations and obtain a system of three equations for θ, ϕ and ψ. They may be written as

$$M\ddot{\boldsymbol{\theta}} + \boldsymbol{P}_\theta(\boldsymbol{\theta}, \dot{\boldsymbol{\theta}}) = \mathbf{0} \tag{39}$$

where $\ddot{\boldsymbol{\theta}} = (\ddot{\theta}, \ddot{\phi}, \ddot{\psi})^{\mathrm{T}}$ and M is a symmetric matrix. The explicit expansion of (39) is given in appendix (A.3). Using *Mathematica*, the system has been shown to be completely equivalent to the system (31).

In general, we can write the Lagrangian in the form

$$\mathcal{L} = \mathcal{L}_0(\theta, \dot{\boldsymbol{\theta}}) + \epsilon\mathcal{L}_1(\theta, \psi, \dot{\boldsymbol{\theta}})$$

where $\mathcal{L}_0$ is the Lagrangian for the integrable symmetric system and $\epsilon = (I_2 - I_1)/I_1$ is the *asymmetry parameter*. This provides a basis for a perturbation analysis when ϵ is small, which will not be undertaken here but will be the subject of future work.

6. Numerical experiments

The numerical integration of the equations is delicate, as there is a singularity of the coordinate system when $\theta = 0$, and significant errors may result from this. To be sure of reliable numerical results, we used a routine of eighth-order accuracy, ODE87, coded by Vasiliy Govorukhin (http://www.mathworks.com/matlabcentral/), which is a realization of the formulae of Prince and Dorman [14]. With this method, invariants of the motion remained constant to high accuracy. To further confirm the robustness of the numerics, we coded both sets of equations, the system (31) in terms of $(\dot{\boldsymbol{\theta}}, \dot{\boldsymbol{\omega}})$ and the system (39) in terms of $(\dot{\boldsymbol{\theta}}, \ddot{\boldsymbol{\theta}})$, and compared the results. Furthermore, we verified the MATLAB coding by an independent coding in *Mathematica*. Finally, the results presented below were checked for convergence by varying the error tolerance. We can therefore be confident in the reliability of the numerical results.

Unless otherwise stated, the numerical values of the parameters are set as follows: gravity $g = 9.87$, unit mass, unit radius, centre of mass off-centring $a = 0.05$, moments of inertia $I_1 = 0.35$ and $I_3 = 0.4$. Some initial conditions will not be varied in the various simulations; these are $\theta_0 = 0.95\pi$, $\dot{\theta}_0 = 0$ and $\phi_0 = 0$.

6.1. The consequence of asymmetry

We first compare the numerical solution of equations (31) for the symmetric case $I_1 = I_2$ and for a case of slight asymmetry. The solutions are for 1500 time units and the initial conditions are, in each case, $\theta_0 = 0.95\pi$, $\phi_0 = \psi_0 = 0$, $\omega_{1,0} = 0$, $\omega_{2,0} = 0.001$, $\omega_{3,0} = -0.001$. Figure 5 (top left panel) shows the trajectory of the point of contact for the symmetric case $I_1 = I_2$. The azimuthal angle increases regularly and steadily for each cycle of rocking motion. This is confirmed by figure 5, top right panel, which shows ϕ at the points where θ reaches a maximum. For the solution shown in the bottom panels of figure 5, the only difference is an increase of 0.1% in the inertial moment about $\boldsymbol{\jmath}$, so that $\epsilon = 10^{-3}$. The bottom left panel shows the trajectory of the point of contact: the precession is no longer uniform. The azimuthal angle alternately increases and decreases (figure 5, bottom right panel). We see that there is recession, with a period much longer than that of the rocking motion. Thus, a minute change in the mass distribution of the body, that changes the inertial structure slightly and breaks the symmetry $I_1 = I_2$, has a dramatic effect on the character of the motion.
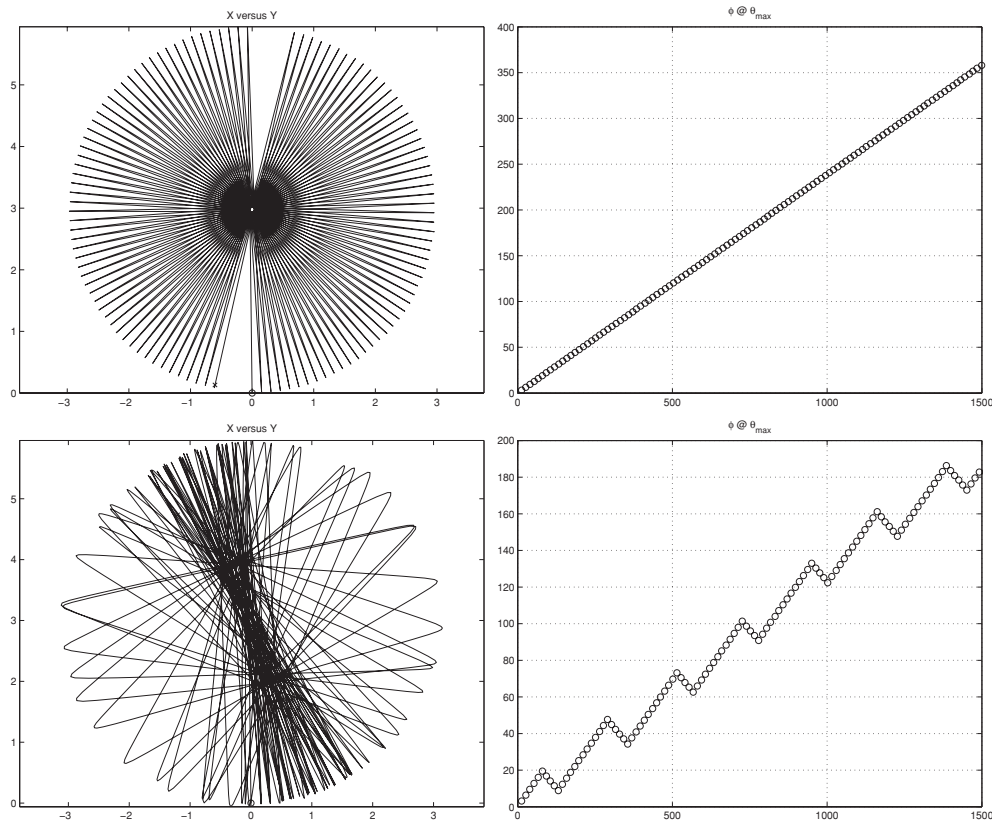
Figure 5. Top left: trajectory of the point of contact for the solution for the symmetric case $I_1 = I_2$. Top right: ϕ versus θ_{max} for the symmetric case. Bottom left and right: corresponding solution for the asymmetric case $I_2 = 1.001I_1$.

6.2. Stability of rocking motion

We initiate the motion from a stationary state with $\omega(0) = 0$ and $\theta(0) = 0.95\pi$. Clearly, a symmetric body started in this configuration would execute pure rocking motion, passing repeatedly through the equilibrium position, with ϕ and ψ remaining constant (apart from jumps of π due to the coordinate singularity at $\theta = 0$). For the asymmetric body, the solution depends on the initial angle $\psi(0) = \psi_0$. As before, we assume that the asymmetry is slight, with $I_2 = 1.001I_1$.

The trajectory of the point of contact of the rock'n'roller is shown in figure 6 for ψ_0 in the set $\{\pi/100, \pi/8, \pi/4, 3\pi/8, 3.9\pi/8, \pi/2\}$. All integrations are for 1000 time units. We see that the motion precesses through an angle $\Phi = \phi_{max} - \phi_{min}$ that depends sensitively on the initial phase ψ_0. It appears that the relationship

$$\Phi = \pi - 2\psi_0 \qquad \text{for} \quad \psi_0 \in (0, \pi)$$

is satisfied, at least approximately.

The cases $\psi_0 = 0$ and $\psi_0 = \pi/2$ correspond to pure rocking about the principal axes with moments of inertia I_2 and I_1 respectively. Motion close to pure rocking about the I_1 axis is stable (figure 6(E)) while that starting close to the I_2 axis changes dramatically, precessing

(A) $\psi_0 = \pi/100$ (B) $\psi_0 = \pi/8$ (C) $\psi_0 = \pi/4$

(D) $\psi_0 = 3\pi/8$ (E) $\psi_0 = 3.9\pi/8$ (F) $\psi_0 = \pi/2$
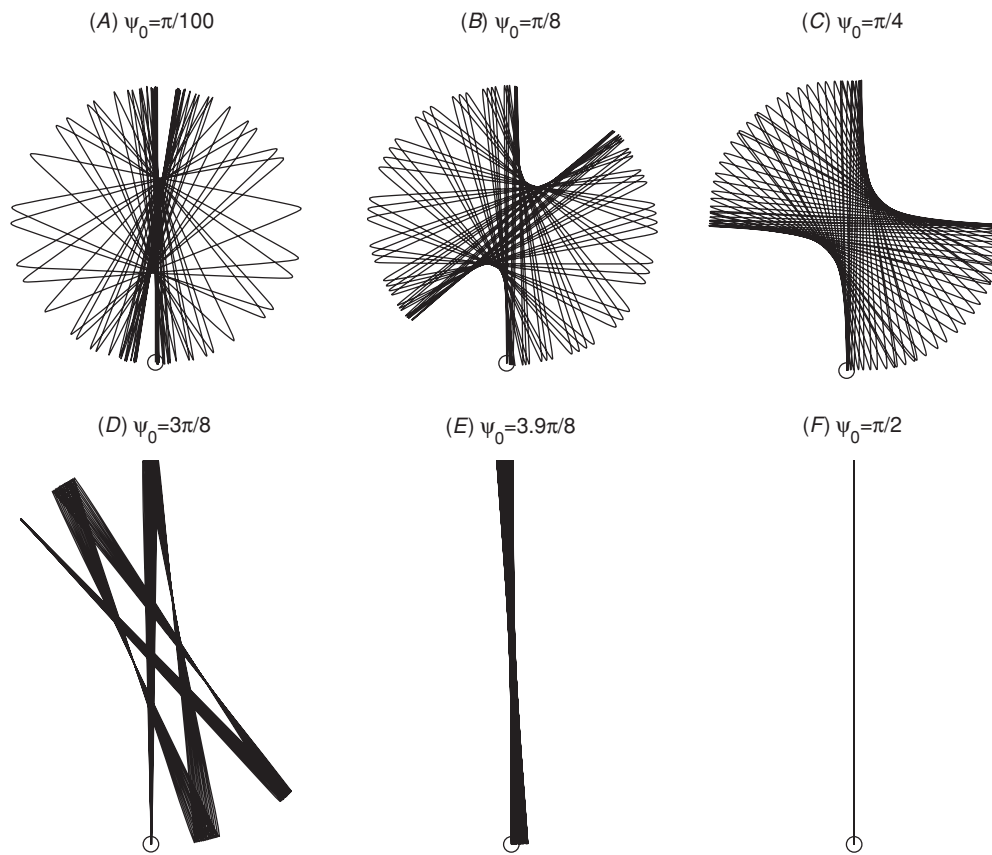
Figure 6. Trajectory of the point of contact in the XY-plane for the initial phase angle $\psi_0 \in \{\pi/100, \pi/8, \pi/4, 3\pi/8, 3.9\pi/8, \pi/2\}$. All integrations are for 1000 time units. The small circles indicate the starting position in each case.

through almost $180°$ (figure 6(A)). We recall the classical result for free motions of a rigid body with $I_1 < I_2 < I_3$, where rotation about the I_2 axis is unstable whereas rotations about the I_1 and I_3 axes are stable.

In general we expect the trajectory to be dense in the domain of angle Φ spanned by the solution. However, KAM theory [1, 13] suggests that for exceptional initial conditions the solution is periodic. The character of the solution for $\psi_0 = 3\pi/8$ appears to be close to a periodic solution (figure 6(D)). Searching in the neighbourhood of this solution, we found that when $\psi_0 = 2.965\pi/8$ the trajectory becomes periodic, repeatedly tracing out the same track, some 15 times in 1000 s. Solutions of this nature, whose trajectories span a set of measure zero, are a signature of integrability.

6.3. Recession and criticality

We now present a numerical study of reversals based on the theory of criticality described in section 2.5. In all cases, the numerical experiments consist of releasing the rock'n'roller at an angle $\theta_0 = 0.95\pi$, with $\dot{\theta}_0 = 0$ and with an angle $\psi_0 = \pi/4$ half-way between the body's principal axes. The system (31) is integrated numerically for 200 time units, using
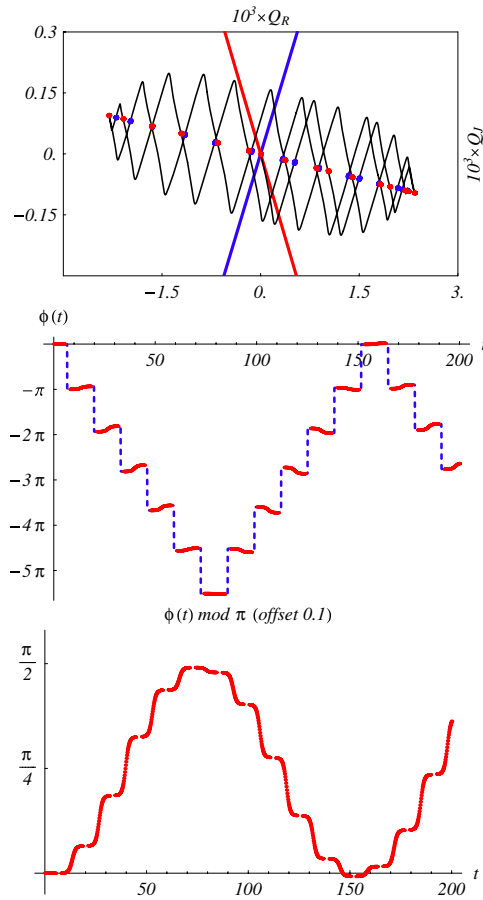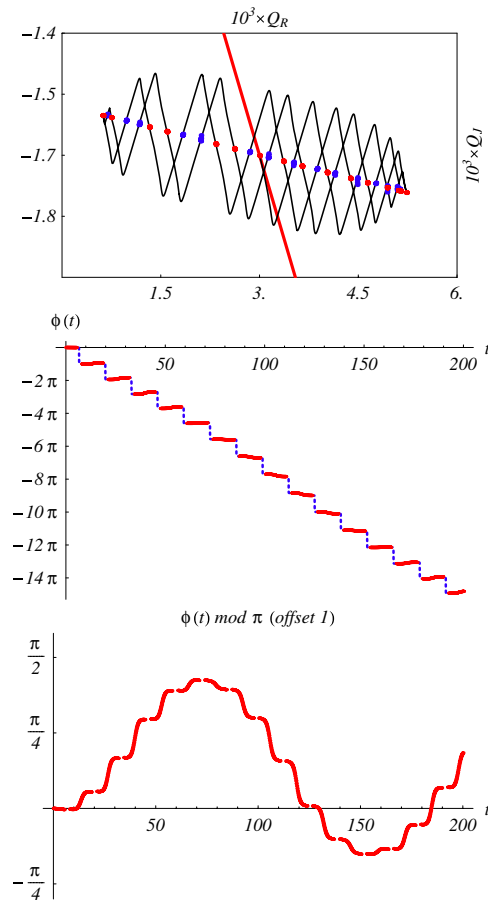
17

Figure 7. Top frame: orbit in the (Q_R, Q_J)-plane for 200 time units. Middle frame: azimuth angle $\phi(t)$. Bottom frame: visible angle $\phi(t) \pmod \pi$ sampled when $\theta \geqslant 0.5\theta_0$. Initial conditions $Q_R = 0, Q_J = 0$. For full details, see the text.

an adaptive *Mathematica* code (stiffness-switching method) with 11th order accuracy. The results are insensitive to resolution improvements. We monitor energy conservation point wise and confirm that the relative error is less than 10^{-10}. Routh's and Jellett's quantities are computed in post-processing.

In figures 7, 8 and 9 all parameters are identical except for the initial conditions. In all three cases, $\theta_0 = 0.95\pi, \dot\theta_0 = 0, \phi_0 = 0, \psi_0 = \pi/4$. Parameter values are $a = 0.05, g = 9.87, I_3 = 2/5, I_1 = (1 - 5a/2)I_3, \epsilon = 10^{-3}$. The top frame in each case shows the orbit in the (Q_R, Q_J)-plane for 200 time units (zigzagging bounded curve (black)). In all three cases, the orbit starts at a point on one of the critical lines and begins moving to the bottom right, subsequently alternating between adjacent critical regions. The straight lines from top left to bottom right (red online) denote the critical line $Q_J = Q_{J,\pi}^{\text{crit}}$, useful for visible angle reversal. The straight lines from bottom left to top right (blue online) denote the critical line $Q_J = Q_{J,0}^{\text{crit}}$, useful for full angle reversal. Dots correspond to instances when $\theta(t)$ is near the turning points: (red online) dots denote $\theta \geqslant 0.99\theta_0$ (near turning point θ_X) and (blue online) dots denote $\theta < 0.005\theta_0$ (near turning point θ_N). The middle frame

18

Figure 8. Top frame: orbit in the (Q_R, Q_J)-plane for 200 time units. Middle frame: azimuth angle $\phi(t)$. Bottom frame: bisible angle $\phi(t)$ (mod π) sampled when $\theta \geqslant 0.5\theta_0$. Initial conditions $Q_R = 0.0030$, $Q_J = Q_{J,\pi}^{\mathrm{crit}} \approx -0.0017$. For full details, see the text.

in each case shows the azimuth angle $\phi(t)$. Solid lines (red online) denote instances when $\theta \geqslant 0.5\theta_0$ and dashed lines (blue online) denote instances when $\theta < 0.5\theta_0$. The bottom frames show the visible (half) angle $\phi(t)$ (mod π) sampled when $\theta \geqslant 0.5\theta_0$.

In figure 7, the initial velocities are $\dot{\phi}_0 = \dot{\psi}_0 = 0$. The motion remains close to the centre $Q_R = Q_J = 0$, i.e. close to pure rocking (the black zigzagging orbit in a top frame). The system alternates between regions I and III, spending approximately five periods of rocking motion in each region. Consequently, both full-angle reversal (middle frame) and visible angle reversal (bottom frame) can be observed. This case corresponds exactly to case (C) in figure 6.

In figure 8, the initial conditions are right on the critical line $Q_J = Q_{J,\pi}^{\mathrm{crit}}$: the initial velocities are $\dot{\phi}_0 = -0.002$ and $\dot{\psi}_0 = 0.002$. The orbit is very similar in shape and size to the orbit in the previous case. We observe two critical crossings between region I and region IV, corresponding to visible angle reversals (bottom frame). There is no full angle reversal (middle frame).
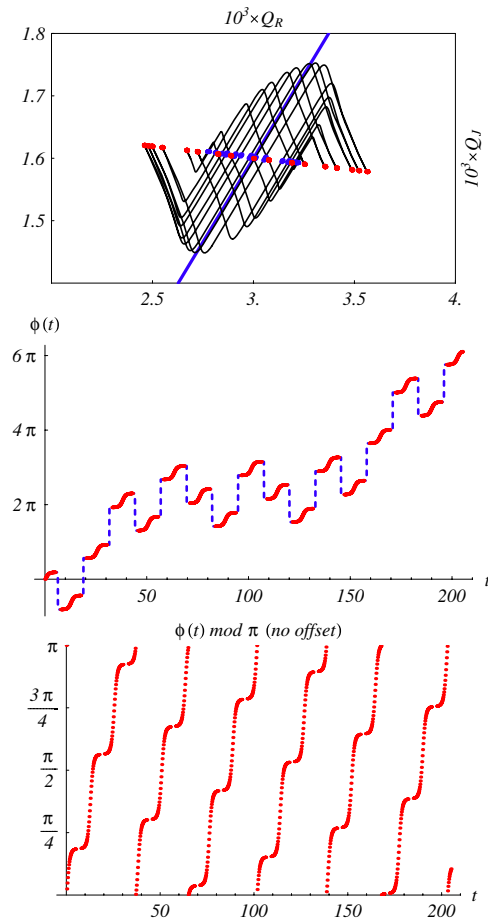
19

Figure 9. Top frame: orbit in the (Q_R, Q_J)-plane for 200 time units. Middle frame: azimuth angle $\phi(t)$. Bottom frame: visible angle $\phi(t)$ (mod π) sampled when $\theta \geqslant 0.5\theta_0$. Initial conditions $Q_R = 0.0030$, $Q_J = Q_{J,0}^{\text{crit}} \approx 0.0016$. For full details, see the text.

In figure 9, the initial conditions are right on the critical line $Q_J = Q_{J,0}^{\text{crit}}$: the initial velocities are $\dot{\phi}_0 = 0.379$ and $\dot{\psi}_0 = 0.378$. The orbit differs in shape from the ones seen above and its horizontal dimension is three times smaller. We observe 11 critical crossings between region I and region II, corresponding to full angle reversals (middle frame). There is no visible angle reversal (bottom frame).

We note in each of the three cases that, regardless of the apparent complexity of the orbits, when the system is near one of the turning points ($\theta = \theta_X(t_j)$, (red online) dots; $\theta = \theta_N(t_j)$, (blue online) dots), the points (Q_R, Q_J) are distributed along a straight line (top frame in each case). In figure 10 a plot is shown combining the orbits of the three initial conditions used in figures 7, 8 and 9, in order to compare their distribution and extent in the plane (Q_R, Q_J).

It is evident from the above that the criticality criterion is a useful description of both full angle and visible angle reversals. One just needs to initialize the system near a critical line and the dynamics will do the rest. However, we do not yet have an explanation for the extent of the orbit, so our method is only descriptive and cannot predict, for example, the number of
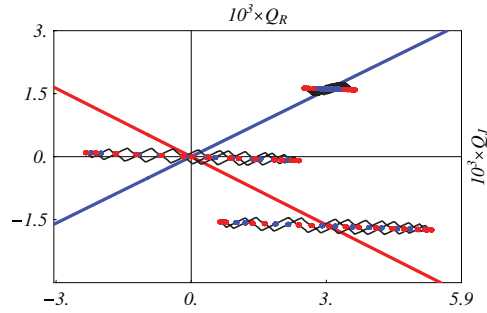
Figure 10. Combined plot of orbits for the three initial conditions described in figures 7, 8 and 9.
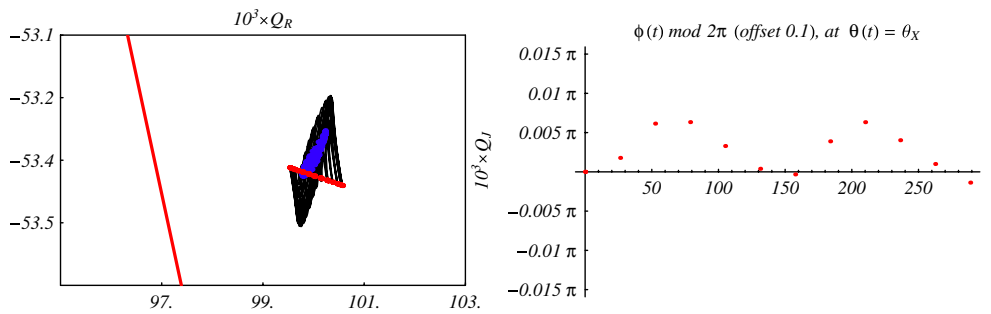

Figure 11. Left frame: high-Q_R reversal orbit, predicted by the asymptotic theory. Colour code as shown in figure 7. Right frame: visible angle ϕ mod 2π, sampled at times t_j when $\theta(t_j)$ attains its maximum value $\theta_X(t_j)$.

rocking cycles executed in each critical region. Forthcoming work should be dedicated to this subject.

Regarding visible angle reversals, we have found that these cease to be observed if the initial (Q_R, Q_J) is chosen far enough from the origin (keeping all other initial conditions fixed). This can be understood from the fact that the asymptotic Laurent expansion in (25) is valid only near $\theta = \pi$, but the maximum attainable $\theta(t)$ is bounded, from energy conservation, by θ_0, which is strictly less than π. From the analysis given in section 2.6, and equation (27), it follows that the necessary condition for validity of the Laurent expansion becomes $Q_R \leqslant 0.1$ for the present choice of parameters and initial conditions, where we have used the observational estimate (from figure 10) of 0.001 for the orbit extension along the Q_R-axis. We have checked that there is indeed reversal for $Q_R = 0.1$ (see figure 11, left frame). It is important to mention that at this relatively high value of Q_R (and correspondingly high angular velocity) the lowest-order Laurent asymptotic expansion given in (25) needs to be improved. As a result, the simple interpretation of reversals in terms of critical crossings and changes of sign of $\dot{\phi}$ will change slightly. In practice, to observe recession in this limiting case, it is necessary to offset slightly the initial condition in the plane (Q_R, Q_J), to a point above the critical line $Q_J = Q_{J,\pi}^{\mathrm{crit}}$. The resulting orbit remains in region I so that there is no change in sign of $\dot{\phi}(t_j)$. However, the visible precession angle $\Delta\phi(t_j)$ (mod 2π), being determined by an integral in time, can and does have reversals (figure 11, right frame).

7. Conclusion

Experiments show that the recession, or reversal of precession, is a robust feature of the motion of the physical rock'n'roller. Analysis has confirmed that for a perfectly symmetric body with $I_1 = I_2$, this behaviour is impossible. However, even the slightest breaking of this inertial symmetry (i.e. a small nonzero value of $\epsilon = (I_2 - I_1)/I_1$) is sufficient to change the character of the solution profoundly, allowing entirely new types of motion. Physical experiments and numerical results show that the reversal angle $\Phi = \phi_{max} - \phi_{min}$ depends sensitively on the initial conditions. For motion that is initially close to pure rocking, the angle Φ can be controlled by the choice of the initial phase angle ψ_0. A rigourous analytical demonstration of this result is outstanding.

The symmetric equations are integrable, with three invariants: the total energy E, Jellett's quantity Q_J and Routh's quantity Q_R. In the asymmetric case, only one of the above three quantities is conserved, namely the total energy. We present an analysis of recession based on the existence of critical lines dividing the (Q_R, Q_J)-plane into four dynamically disjoint regions. We prove that recession is directly related to the lack of conservation of Jellett's and Routh's quantities, by identifying individual reversals as crossings of the orbit $(Q_R(t), Q_J(t))$ through the critical lines. The criticality criterion allows one to produce a family of initial conditions so that the system will exhibit recession.

In the asymmetric case, there remains an underlying geometric symmetry—invariance under change of the azimuthal angle ϕ—so it is arguable that another dynamical invariant exists. Note that Borisov and Mamaev [2] indicate in their table 1 that the quantity $M^2 - 2Kr^2$ is conserved in the asymmetric case (where M is the angular momentum about the contact point); however, this is only true in the absence of gravity. In the realistic case where gravity is present, this additional integral (if it exists) remains to be found.

There is apparently a slow period of the orbit $(Q_R(t), Q_J(t))$. This suggests multi-scale analysis as an appropriate technique for analysis of this problem. For a small asymmetry parameter ϵ, the problem may be formulated as a perturbed integrable Lagrangian system, and is amenable to standard asymptotic analysis. This will be the subject of future work. KAM theory [1, 13] would indicate that certain aspects of integrability should apply to the weakly asymmetric rock'n'roller. However, the question of the general integrability of the system remains open.

Appendix

A.1. The basic parameters of the rock'n'roller

Let us assume that the body consists of a homogeneous material of uniform density, and that its mass and radius are both unity. We denote by Θ the co-latitude of the polar cap that is removed to construct the rock'n'roller. All the dynamical parameters are determined once this angle is fixed. We define the distance from the geometric centre to the centre of the planar face of the body:

$$d = \cos\Theta.$$

The volume of the body is then

$$V = \pi \left(\frac{2}{3} + d - \frac{1}{3}d^3 \right).$$

The off-set of the mass centre from the geometric centre is

$$a = \frac{\pi}{4} \left(\frac{d^2(2 - d^2) - 1}{V} \right).$$

The moments of inertia about the geometric centre are

$$I_3' = \frac{\pi}{2} \left(\frac{\frac{8}{15} + d - \frac{2}{3}d^3 + \frac{1}{5}d^5}{V} \right), \qquad I_1' = \pi \left(\frac{\frac{4}{15} + \frac{1}{4}d + \frac{1}{6}d^3 - \frac{3}{20}d^5}{V} \right).$$

By means of the parallel axis theorem [18], the moments of inertia about the centre of mass are

$$I_3 = I_3' \qquad I_1 = I_1' - a^2.$$

For the actual rock'n'roller shown in figure 1, the polar angle is $\Theta \approx 53°$. Thus $d = 0.6$, giving the (nondimensional) parameter values

$$a = 0.085 \qquad I_1 = 0.362 \qquad I_3 = 0.42.$$

For our numerical experiments we used the values $a = 0.05$, $I_1 = 0.35$ and $I_3 = 0.4$.

A.2. The equations for the symmetric rock'n'roller

The equations for the symmetric case $I_1 = I_2$ were given in section 2.1. The details are given here. Taking the cross-product of $\boldsymbol{r}$ with the momentum equation (5) gives

$$\boldsymbol{r} \times \dot{\boldsymbol{v}} + \boldsymbol{r} \times (\boldsymbol{\Omega} \times \boldsymbol{v}) = \boldsymbol{r}F = \boldsymbol{r} \times \boldsymbol{W} - \boldsymbol{G}. \tag{A.1}$$

Noting that $\dot{\theta} = \omega_1$, the acceleration in $\boldsymbol{i}'\boldsymbol{j}'\boldsymbol{k}'$-components is

$$\dot{\boldsymbol{v}} = (f\dot{\omega}_2' - s\dot{\omega}_3', -f\dot{\omega}_1', s\dot{\omega}_1') + \left(-\omega_1'(s\omega_2' + c\omega_3'), s\omega_1'^2, c\omega_1'^2 \right).$$

It follows that

$$\boldsymbol{r} \times \dot{\boldsymbol{v}} = [(s^2 + f^2)\dot{\omega}_1', f^2\dot{\omega}_2' - fs\dot{\omega}_3', -fs\dot{\omega}_2' + s^2\dot{\omega}_3')$$
$$+ (as\omega_1'^2, -f\omega_1'(s\omega_2' + c\omega_3'), s\omega_1'(s\omega_2' + c\omega_3'))]$$

and

$$\boldsymbol{r} \times (\boldsymbol{\Omega} \times \boldsymbol{v})\boldsymbol{r} = (\boldsymbol{r} \cdot \boldsymbol{v})\boldsymbol{\Omega} - (\boldsymbol{r} \cdot \boldsymbol{\Omega})\boldsymbol{v}$$
$$= -(s^2 + cf)(\omega_2'/s)(f\omega_2' - s\omega_3', -f\omega_1', s\omega_1').$$

Moreover,

$$\boldsymbol{r} \times \boldsymbol{W} = -gas\boldsymbol{i}'.$$

Using these expressions in (A.1) we get

$$G_1 = G_1^0 - (s^2 + f^2)\dot{\omega}_1'$$
$$G_2 = G_2^0 - (f^2\dot{\omega}_2' - fs\dot{\omega}_3')$$
$$G_3 = G_3^0 - (s^2\dot{\omega}_3' - fs\dot{\omega}_2')$$

where, defining the height of the centre of mass as $h = 1 - ac$,

$$G_1^0 = -\left[as\omega_1'^2 - h(f\omega_2' - s\omega_3')\omega_2'/s\right] - gas$$
$$G_2^0 = -[-f\omega_1'(s\omega_2' + c\omega_3') + hf\omega_1'\omega_2'/s]$$
$$G_3^0 = -[s\omega_1'(s\omega_2' + c\omega_3') - h\omega_1'\omega_2'].$$

23

We can now substitute for G in (8) to obtain

$$\begin{aligned}
[I_1 + (s^2 + f^2)]\dot{\omega}_1' &= -(I_3\Omega_2\omega_3' - I_1\Omega_3\omega_2') + G_1^0 \equiv P_1 \\
[I_1 + f^2]\dot{\omega}_2' + [-fs]\dot{\omega}_3' &= -(I_1\Omega_3\omega_1' - I_3\Omega_1\omega_3') + G_2^0 \equiv P_2 \\
[-fs]\dot{\omega}_2' + [I_3 + s^2]\dot{\omega}_3' &= +G_3^0 \equiv P_3.
\end{aligned} \tag{A.2}$$

The first equation immediately gives the evolution of ω_1':

$$\dot{\omega}_1' = \frac{P_1}{I_1 + s^2 + f^2} \equiv S_1.$$

The second and third equations can be written as

$$\begin{bmatrix} I_1 + f^2 & -fs \\ -fs & I_3 + s^2 \end{bmatrix} \begin{pmatrix} \dot{\omega}_2' \\ \dot{\omega}_3' \end{pmatrix} = \begin{pmatrix} P_2 \\ P_3 \end{pmatrix}.$$

The matrix is nonsingular, with determinant $\Delta = (I_1 I_3 + I_1 s^2 + I_3 f^2)$ and inverse

$$\begin{pmatrix} \dot{\omega}_2' \\ \dot{\omega}_3' \end{pmatrix} = \frac{1}{\Delta} \begin{bmatrix} I_3 + s^2 & fs \\ fs & I_1 + f^2 \end{bmatrix} \begin{pmatrix} P_2 \\ P_3 \end{pmatrix} \equiv \begin{pmatrix} S_2 \\ S_3 \end{pmatrix}.$$

The complete system of equations for the angular variables is now obtained:

$$\begin{aligned}
\dot{\theta} &= \omega_1', & \dot{\phi} &= \omega_2'/s, & \dot{\psi} &= \omega_3' - (c/s)\omega_2', \\
\dot{\omega}_1' &= S_1, & \dot{\omega}_2' &= S_2, & \dot{\omega}_3' &= S_3.
\end{aligned}$$

This system provides six equations for the six variables $\{\theta, \phi, \psi, \omega_1', \omega_2', \omega_3'\}$.

A.3. The Euler–Lagrange equations

The Lagrange equations arising from (37) may be written as

$$M\ddot{\boldsymbol{\theta}} + \boldsymbol{P}_\theta(\boldsymbol{\theta}, \dot{\boldsymbol{\theta}}) = \boldsymbol{0} \tag{A.3}$$

where $\ddot{\boldsymbol{\theta}} = (\ddot{\theta}, \ddot{\phi}, \ddot{\psi})^{\mathrm{T}}$. The symmetric matrix M is defined as

$$M = \begin{bmatrix} I_1\chi^2 + I_2\sigma^2 + a^2 s^2 + h^2 & (I_1 - I_2)s\sigma\chi & 0 \\ (I_1 - I_2)s\sigma\chi & (I_1\sigma^2 + I_2\chi^2 + a^2)s^2 + I_3 c^2 & I_3 c + as^2 \\ 0 & I_3 c + as^2 & I_3 + s^2 \end{bmatrix}$$

and the vector $\boldsymbol{P}_\theta = (P_\theta, P_\phi, P_\psi)$ has components:

$$\begin{aligned}
P_\theta ={}& [as]\dot{\theta}^2 + [-(I_1\sigma^2 + I_2\chi^2 - I_3)sc + has]\dot{\phi}^2 + [-(I_1 - I_2)2\sigma\chi]\dot{\theta}\dot{\psi} \\
&+ [(I_1 - I_2)s(\chi^2 - \sigma^2) + I_3 s + hs]\dot{\phi}\dot{\psi} + gas, \\
P_\phi ={}& [(I_1 - I_2)c\sigma\chi]\dot{\theta}^2 + [(I_1\sigma^2 + I_2\chi^2 - I_3)2sc + (2ac - 1)as]\dot{\theta}\dot{\phi} \\
&+ [(I_1 - I_2)s(\chi^2 - \sigma^2) - I_3 s + asc]\dot{\theta}\dot{\psi} + [(I_1 - I_2)2s^2\sigma\chi]\dot{\phi}\dot{\psi}, \\
P_\psi ={}& [(I_1 - I_2)\sigma\chi]\dot{\theta}^2 + [-(I_1 - I_2)s^2\sigma\chi]\dot{\phi}^2 \\
&+ [-((I_1 - I_2)(\chi^2 - \sigma^2) + I_3)s + (2ac - 1)s]\dot{\theta}\dot{\phi} + [sc]\dot{\theta}\dot{\psi}.
\end{aligned}$$

Now (A.3) may be solved for $(\boldsymbol{\theta}(t), \dot{\boldsymbol{\theta}}(t))$. It has been confirmed, using *Mathematica*, that the system (39) is completely equivalent to the system (31).

References

[1] Berry M V 1978 Regular and irregular motion *AIP Conf. Proc.* **46** 16–120 (Reprinted)
 MacKay R S and Meiss J D 1987 *Hamiltonian Dynamical Systems* (Bristol: Hilger) pp 27–53
[2] Borisov A V and Mamaev I S 2002 Rolling of a rigid body on a plane and a sphere. Hierarchy of dynamics. *Reg. Chaotic Dyn.* **7** 177–200
[3] Chaplygin S A 1903 On a sphere rolling on a horizontal plane *Math. Collect. Moscow Math. Soc.* **24** 139–68
 Chaplygin S A 2002 *Reg. Chaotic Dyn.* **7** 131–48 DOI: 10.1070/RD2002v007n02ABEH000200 (English transl.)
[4] Cushman R 1998 Routh's Sphere *Rep. Math. Phys.* **42** 47–70 (*Proc. Pacific. Inst. Math. Sci., Workshop on Nonholonomic Constraints in Dynamics*)
[5] Duistermaat J J 2004 Chaplygin's sphere arXiv:math.DS/0409019 v1
[6] Flannery M R 2005 The enigma of nonholonomic constraints *Am. J. Phys.* **73** 265–72
[7] Gray C G and Nickel B G 2000 Constants of the motion for nonslipping tippe tops and other tops with round pegs *Am. J. Phys.* **68** 821–8
[8] Hand L N and Finch J D 1998 *Analytical Mechanics* (Cambridge: Cambridge University Press) 575pp
[9] Holm D D 2008 *Geometric Mechanics. Part I: Dynamics and Symmetry. Part II: Rotating, Translating and Rolling* (London: Imperial College Press)
[10] Kilin A A 2001 The dynamics of Chaplygin ball: the qualitative and computer analysis *Reg. Chaotic. Dyn.* **6** 291 DOI: 10.1070/RD2001v006n03ABEH000178
[11] Landau L D and Lifshitz E M 1976 *Course of Theoretical Physics, Vol. 1: Mechanics* 3rd edn (Amsterdam: Elsevier) 170pp
[12] Montaldi J and Ratiu T 2005 *Geometric Mechanics and Symmetry: the Peyresq Lectures (London Mathematical Society Lecture Note Series* 306*)* (Cambridge: Cambridge University Press) 402pp
[13] Edward O 2002 *Chaos in Dynamical Systems* 2nd edn (Cambridge: Cambridge University Press) 385pp
[14] Prince P J and Dorman J R 1981 High order embedded Runge–Kutta formulae *J. Comput. Appl. Math.* **7** 67–75
[15] Routh E J 1905 *A Treatise on the Dynamics of a System of Rigid Bodies, Part II: The Advanced Part* 6th edn (New York: Macmillan) (Reprinted by Dover, New York, 1955)
[16] Schneider D A 2002 Non-holonomic Euler–Poincare equations and stability in Chaplygin's Sphere *Dyn. Syst.* **17** 2 87–130
[17] Jinglai S, Schneider D A and Bloch A M 2003 Controllability and Motion Planning of a Multibody Chaplygin's Sphere and Chaplygin's Top *Report No 43 (Institut Mittag-Leffler. Royal Swedish Academy Sci)*
[18] Synge J L and Griffith B A 1959 *Principles of Mechanics* (New York: McGraw-Hill) 552pp
[19] Ueda T, Sasaki K and Watanabe S 2005 Motion of the tippe top: gyroscopic balance condition and stability (http://arxiv.org/pdf/physics/0507198)
[20] Whittaker E T 1937 *A Treatise on the Analytical Dynamics of Particles and Rigid Bodies* 4th edn (Cambridge: Cambridge University Press)